Published in ChemPhysChem 7, issue 2, 514-523, 2006
which should be used for any reference to this work

Enantiodiscrimination between an *N*-Acetyl-L-cysteine SAM and Proline: An In Situ Spectroscopic and Computational Study**

Marco Bieri and Thomas Bürgi*[a]

A combination of attenuated total reflection infrared (ATR-IR) and modulation excitation spectroscopy (MES) is used to study the enantiodiscriminating interactions between proline and a chiral, self-assembled monolayer (SAM) of N*-acetyl-*L*-cysteine on gold. The* N*-acetyl-*L*-cysteine SAM consists of a mixture of protonated and deprotonated molecules. Whereas both species are influenced by adsorbed proline, only the deprotonated molecules are involved in enantiodiscrimination. Density functional theory (DFT) calculations reveal that electrostatics dominates the interaction between the two molecules. By modulating the absolute configuration of proline over the chiral SAM, and a subsequent phase-sensitive detection of the periodically varying signals in the ATR-IR spectra, the small spectral differences between the diastereomeric complexes are spotted. The resulting difference spectrum is in qualitative agreement with the spectrum predicted by the DFT calculations.*

Introduction

Chiral surfaces and interfaces play an important role in various fields of modern technology, such as in chromatography[1] and heterogeneous enantioselective catalysis.[2,3] Despite the practical interest in chiral interfaces, the former is also more and more the subject of fundamental research.[4–22] Chiral interfaces can distinguish between enantiomers of a chiral compound,[23–25] a property which becomes increasingly important, since separation, selective production, and detection of enantiomers is a fast-growing market. At the origin of this trend is the biological homochirality on earth, which, in turn, may even have been caused by chiral surfaces.[26,27]

The rational design of the fundamental property of chiral interfaces, namely their ability to distinguish between adsorbed enantiomers, goes hand in hand with the development of powerful techniques, which can, on a molecular level, give information on the origin of enantiodiscrimination. The latter is in most cases determined by intermolecular interactions. It is therefore desirable to develop techniques that can, not only quantify enantiodifferentiation, but also shed light on its origin. Such techniques should ideally provide molecular level information and combine (surface-) sensitivity with selectivity for chiral information, a combination of criteria that is difficult to meet simultaneously. Nonlinear optical techniques may turn out to be powerful for the investigation of chiral interfaces.[28–30]

We have recently proposed a method to investigate enantiodiscrimination at chiral solid/liquid interfaces that combines attenuated total reflection infrared (ATR-IR) spectroscopy[31] with modulation excitation spectroscopy (MES).[32,33] The former allows the measurement of infrared spectra of adsorbed molecules in the presence of a solvent. The latter technique uses the periodic stimulation of the investigated system and the phase-sensitive detection (PSD) of the induced response. The PSD leads first of all to an increased sensitivity. In addition, the system under investigation can selectively be questioned by selection of the appropriate stimulation parameter. By choosing the absolute configuration of the probe molecule as the periodic stimulation, the enantiodiscriminating interactions can selectively be spotted, since the infrared spectra of the enantiomers are identical, except when they interact with a chiral environment, which is able to distinguish between them. We have demonstrated the power of the technique by investigating enantiodiscrimination at chiral stationary phases used in chromatography.[34,35]

Chiral self-assembled monolayers (SAMs) are potentially interesting for sensing applications and for separations in microsystems.[24,25,36,37] Very recently, we studied the interaction of proline with a chiral SAM of L-glutathione (GSH, γ-Glu-Cys-Gly) on gold.[38] It could be shown that the GSH SAM can discriminate well between the enantiomers of proline. Upon interaction with proline, the relatively flexible *Y*-shaped GSH molecules changed their conformation on the surface. Herein, we investigate the enantiodiscrimination of *N*-acetyl-L-cysteine (NAC, Scheme 1) SAMs on gold. NAC can be viewed as the anchoring part of GSH, and it has less conformational freedom than the latter. On the basis of the absolute configuration modulation experiments and density functional theory (DFT) calculations, a model for the interactions of proline with the chiral NAC SAM is proposed and it is furthermore shown that the interaction is significantly different from the GSH case.

[a] *M. Bieri, Prof. Dr. T. Bürgi*
Université de Neuchâtel, Institut de Chimie
Rue Emile-Argand 11, 2007 Neuchâtel (Switzerland)
Fax: (+41) 32-718-2511
E-mail: thomas.burgi@unine.ch

[**] *SAM = Self-Assembled Monolayer.*

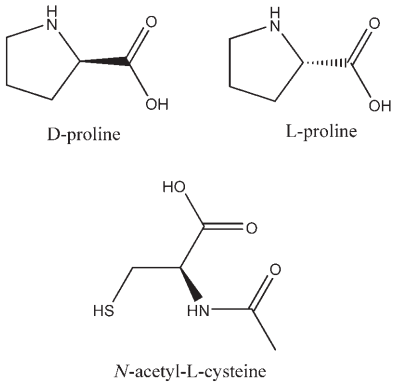

Scheme 1. Structure of proline (top) and *N*-acetyl-L-cysteine (NAC, bottom).

Results and Discussion

DFT Calculations of *N*-Acetyl-L-cysteine and Proline

For a better understanding of the structure of NAC (selector, Scheme 1), proline (selectand, Scheme 1), and their complexes, and to assign the corresponding vibrational spectra, DFT calculations were performed. The conformations with lowest energies found for proline and NAC, are displayed as insets in Figures 1 and 2, respectively. In the case of proline, the energetically most favorable conformation was found to have a hydrogen bond between the carboxylate and the protonated amine.

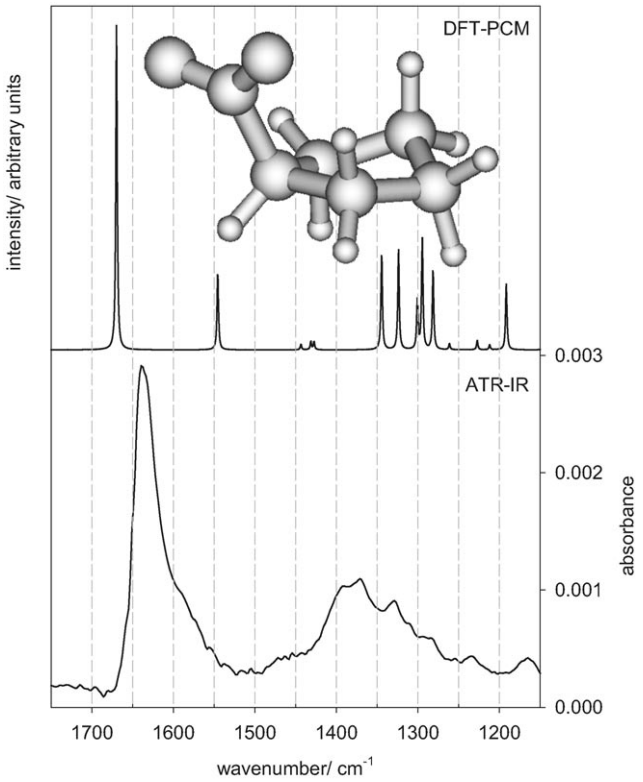

Figure 1. Top) Calculated IR spectrum of proline after convolution with a Lorentzian band shape ($\gamma = 1$ cm^{-1}). The inset shows the conformation of proline (zwitterionic) used for the spectrum calculation. For details concerning the calculation method, see text. Bottom) Experimental ATR-IR spectrum of proline dissolved in ethanol. The phase-resolved (demodulated), spectrum refers to an "L-proline versus ethanol" modulation experiment which consisted of alternately flowing L-proline (about 0.04 M) and ethanol over the bare Ge IRE at a flow rate of 0.5 mL min^{-1} (see the Experimental Section for a description of the modulation experiments). Observed and calculated vibrational bands of proline are listed in Table 1.

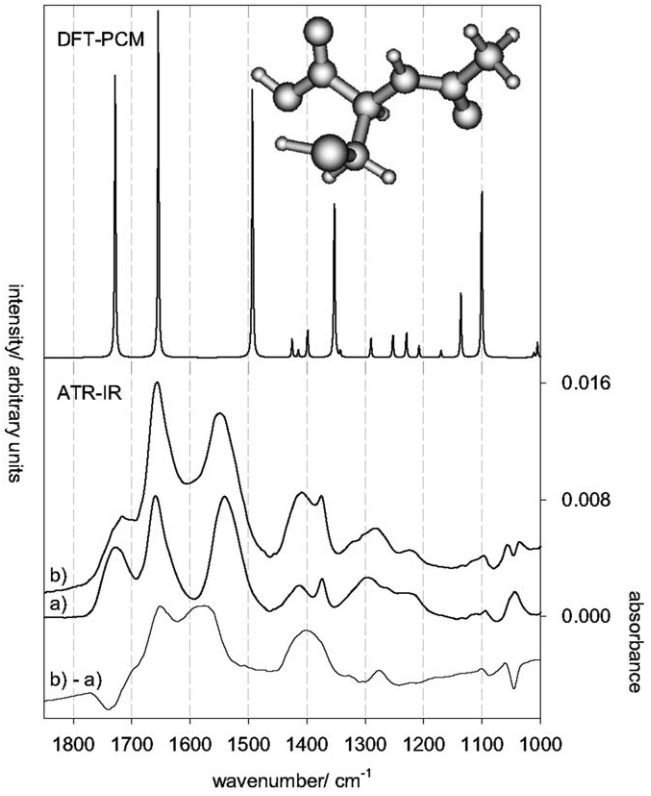

Figure 2. Top) Calculated IR spectrum of NAC. The spectrum was obtained by convoluting the calculated IR intensities with a Lorentzian band shape ($\gamma = 1$ cm^{-1}). The NAC conformation used for the calculation of the spectrum is shown in the inset. See text for details concerning the calculation method. Bottom) Experimental ATR-IR spectra of NAC adsorbed on the gold coated Ge IRE. Spectrum "a" was recorded at the start of the self-assembling process, spectrum "b" recorded about two hours afterwards. The corresponding difference spectrum is "b−a". Typical NAC concentrations were about 0.6 mM for ATR-IR experiments. Experimental and calculated vibrational frequencies of NAC are summarized in Table 1.

In this conformation, the carbon in the ring opposite to the carboxylate group points out of the ring plane in the same direction as the carboxylate (see inset in Figure 1). Another conformation with a slightly higher energy, but similar IR spectrum, has the carbon pointing in the opposite direction with respect to the carboxylate.[38] In the following, the conformation shown in Figure 1 was considered.

For NAC, a *trans* configuration within the rather rigid amide group with (weak) hydrogen bonds between the NH and the carboxylic acid, and between the SH and the carboxylic acid were found to have the lowest energy.

DFT Calculations of a *N*-Acetyl-L-cysteine–D(L)-proline Complex

The interactions between NAC and D- and L-proline, respectively, were studied with the optimized structure of anionic

NAC (see below) as the starting point. D(L)-proline was then allowed to interact with NAC at different sites involving different functional groups: proline–NH_2^+···O=C–amide–NAC, proline–NH_2^+···OOC^-–NAC and proline–COO^-···HN–amide–NAC, were used as prominent examples for interactions. However, among all these possibilities, and not surprisingly, the ionic interactions between the positively charged proline NH_2^+ group and the negatively charged NAC carboxylate COO^- turned out to dominate the interaction strength. To include ionic proline–NAC intermolecular interactions, the conformational space of the complex was further probed by using a Born–Oppenheimer molecular dynamics (BOMD) model[39] with the semi-empirical AM1 Hamiltonian.[40] The trajectory calculation was performed up to about 1.3 ps (ca. 900 steps in each trajectory). For each of the NAC–D(L)-proline complexes, three conformations with low energies of the trajectories were chosen as the starting geometries for structure optimization by DFT. All of the DFT-optimized structures revealed a relative arrangement of NAC and proline as shown in Figure 3a. This configuration is favorable from an electrostatic point of view, since the two negative charges are widely separated and at the same time opposite charges are close, as is schematically indicated in Figure 3a. With the optimized structure of the NAC–L-proline complex at hand, the same procedure was repeated for the NAC-D–proline complex, just by changing the absolute configuration of proline (see Scheme 1 for the configuration of the two enantiomers). The result of the NAC–D-proline structure optimization is displayed in Figure 3b. The analogous ionic interactions between the D-proline NH_2^+ group and the carboxylate COO^- of NAC are possible. The potential energy difference between the two chiral complexes was found to be only about 0.2 kJ mol^{-1}, with the NAC–L-proline complex being energetically more favorable. It should be noted that the structure optimization and vibrational analysis of the complexes were performed using the polarizable continuum model (PCM) model to include solvent (ethanol) effects.

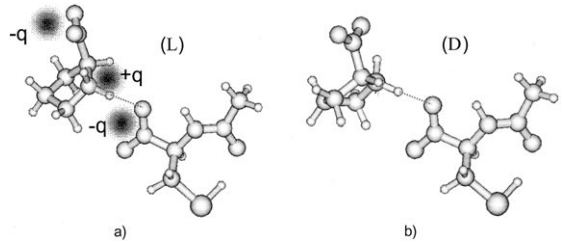

Figure 3. Pictorial representation of the optimized structures of the NAC–L-proline (a) and NAC–D-proline (b) complexes. The complex is determined by ionic proline–NH_2^+···COO^-–NAC intermolecular interactions. In (a), the partially charged groups are schematically indicated with corresponding charge clouds. For details concerning the calculation method, see text.

Characterization of the *N*-Acetyl-L-cysteine SAM (Selectand)

The lower half of Figure 2 shows the ATR-IR spectra recorded during the NAC self-assembling process on gold. Specifically, spectrum "a" was recorded at the beginning of the self-assembling process, whereas spectrum "b" was recorded about two hours afterwards. In the upper half in Figure 2, the calculated vibrational spectrum of NAC in its neutral form (see inset) is displayed, this was obtained by convoluting the calculated IR intensities with a Lorentzian band shape (half width at half maximum, $\gamma = 1$ cm^{-1}). The overall agreement between the calculated and experimentally obtained spectrum is good enough to allow an assignment of the most prominent vibrational bands, which notably are the ν(–COOH) mode at 1727 cm^{-1}, the amide I and amide II vibrations at 1661 and 1539 cm^{-1}, respectively, and the coupled methyl $+ \delta(-CH_2) + \delta(-COH) + \nu(-CO)$ mode at 1375 cm^{-1}. The assignment is summarized in Table 1. However, considering the two ATR-IR spectra depicted in the lower half of Figure 2, significant spectral differences become apparent with time, which are emphasized in the corresponding difference spectrum labeled "b−a". The difference spectrum shows structural changes within the adsorbate layer beside bare mass uptake. The two signals at 1590 and 1400 cm^{-1} are assigned to the

Table 1. Observed vibrational bands (in wavenumbers) of NAC adsorbed on gold, and proline (zwitterionic) dissolved in ethanol.[a]

NAC	Proline	Assignment
static signals		
1727		ν(–COOH)
1661		amide I
1590		ν_{as}(–COO^-)
1539		amide II
1400		ν_s(–COO^-)
1375		methyl $+ \delta(-CH_2) + \delta$(–COH) $+ \nu$(–CO)
phase-resolved signals		
	1637	ν_{as}(–COO^-)
	1570	δ_s(–NH_2) scissoring (appearing as shoulder of band at 1637 cm^{-1})
	1392	ν_s(–COO^-) $+ \delta$(–CH)
	1370	ν_s(–COO^-) $+ \delta$(–CH)
calculated signals		
1729		ν(–COOH)
	1660	ν_{as}(–COO^-)
1655		amide I
	1537	δ_s(–NH_2) scissoring
1494		amide II
1353		methyl $+ \delta(-CH_2) + \delta$(–COH) $+ \nu$(–CO)
	1340	ν_s(–COO^-) $+ \delta$(–CH)
	1300	ν_s(–COO^-) $+ \delta$(–CH)

[a] The static spectrum of NAC is depicted in Figure 2 (spectrum a) and the phase-resolved proline spectrum is displayed in Figure 1 (bottom). Frequencies of calculated NAC and proline vibrations are also included for comparison.

ν_{as}(–COO$^-$) and ν_s(–COO$^-$) vibrations, respectively, which indicates a deprotonation of adsorbed NAC molecules. This deprotonation process is assisted by the interaction of the carboxylic acid group with the Au surface, which acts as a proton acceptor. In a previous work, we have derived the average orientation of NAC molecules within the adsorbate layer at the initial stage of self-assembling.[41] In this orientation analysis, based on the ratio of vibrational band intensities of randomly and oriented molecules from the bulk phase and adsorbed on the Au surface, respectively, a close proximity of the carboxylic acid group to the surface was suggested. Interaction of the carboxylic acid group with the gold surface and deprotonation was furthermore demonstrated for the adsorption of similar molecules, such as L-glutathione[42] and cysteine on gold.[43]

The spontaneous deprotonation of NAC molecules within the SAM was also observed when the adsorption was stopped after about one minute by flowing solvent (ethanol) over the sample. The spectral response clearly revealed deprotonation, which was followed in situ until no variation in the spectra could be detected (about thirty minutes). On the basis of the ratio between the integrated intensities of the carboxylic acid vibrational bands before and after the deprotonation process, we estimate that about 40% of adsorbed NAC molecules undergo a deprotonation. The spectrum recorded at the end of the deprotonation process was found to be very similar to the one shown in Figure 2, recorded two hours after the start of the self-assembling process (spectrum b). We will show later that these two NAC layers, despite the different assembling time and coverage show remarkably similar enantiodiscrimination in the absolute configuration modulation experiments, whereas in the presence of an acid, which prevents deprotonation of adsorbed NAC, the spectral response was completely different in analogous experiments. This suggests that preferentially one of the two ionic forms of NAC present on the surface is involved in the interaction with proline. As ionic interactions are expected to dominate the adsorption of zwitterionic proline under our conditions, which was further confirmed by the DFT calculations, we suggest that the deprotonated NAC on the gold surface is responsible for the observed spectral changes, upon interaction of proline with the NAC SAM, described in the following.

The Analyte Molecule Proline (Selector)

The lower half of Figure 1 shows a (demodulated) ATR-IR spectrum of L-proline in ethanol (recorded over the bare Ge internal reflection elements, IRE). The L-proline spectrum reveals a prominent peak at 1637 cm^{-1} with a shoulder at about 1570 cm^{-1}. In addition, a broad feature composed of several overlapping bands is visible in the region between 1400 and 1300 cm^{-1}. The calculated IR spectrum of proline is shown in the upper half of Figure 1. This spectrum was simulated by convoluting the calculated IR intensities with a Lorentzian band shape using $\gamma = 1$ cm^{-1}. Besides shifts in wavenumber, the overall agreement is good enough to allow an assignment of the most prominent vibrational bands. Specifically, the prominent asymmetric band at 1637 cm^{-1} can be assigned to the ν_{as}(–COO$^-$) vibration with the δ_s (–NH$_2$) scissoring mode at 1570 cm^{-1} appearing as shoulder on the former band. Other vibrational modes of proline are listed in Table 1 and were found to be in agreement with previous reports.[44]

Modulation Experiments and Enantioselective Discrimination

In the lower half of Figure 4, an ATR-IR spectrum of each of the interacting species, that is, NAC adsorbed on the gold coated Ge IRE (selector, represented by ——) and dissolved proline (selectand, represented by ——), respectively, is shown for clarity reasons. In the upper half in Figure 4, the top trace refers to a time-resolved ATR-IR spectrum, which was recorded while flowing L-proline over the NAC SAM. For this experiment, the NAC SAM was allowed to self-assemble for about two hours. This spectrum is thus a superposition of the individual NAC SAM and proline (mainly from the bulk phase) spectra. Note that the reference for this absorption spectrum was recorded before starting the NAC self-assembling. The strongest band in the spectrum at 1637 cm^{-1} is a superposition of the ν_{as}(–COO$^-$) of proline and the amide I vibration of NAC. The phase-resolved, that is, demodulated spectrum of an "L-proline

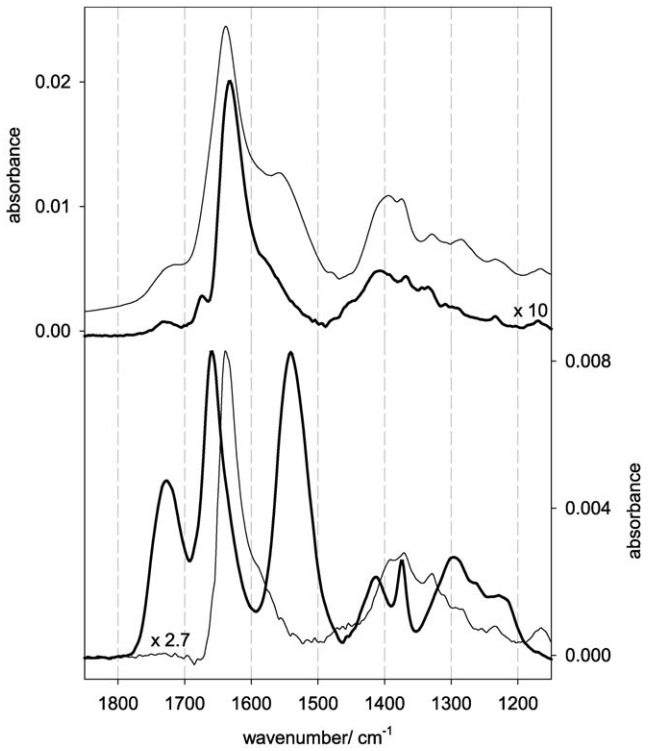

Figure 4. Bottom) ATR-IR spectra of NAC (selector) adsorbed on a gold surface (——) and proline (selectand, ——, scaled by a factor of 2.7) dissolved in ethanol. The two spectra are included for clarity, and are also presented in Figures 1 (proline) and 2 (NAC). Top) A static (time-resolved) ATR-IR spectrum (——) recorded while flowing L-proline over the NAC SAM after about two hours of self-assembling. The reference was taken before SAM formation. A demodulated (phase-resolved) spectrum (——) of an "L-proline versus ethanol" modulation experiment. In this modulation experiment (period $T = 72.4$ s, flow rate 0.5 mL min^{-1}), L-proline (0.04 M) was periodically replaced by ethanol and flowed over the NAC SAM.

versus ethanol" modulation experiment ($T = 72.4$ s, flow rate = 0.5 mL min^{-1}), performed over the NAC modified surface and scaled by a factor of ten, is depicted by —— in the upper half in Figure 4. Obviously (and not surprisingly) this spectrum is dominated by the bulk-phase proline vibrational bands (compare to the proline spectrum in the lower half in Figure 4). It should be emphasized here that only bands that are periodically changing with time owing to the stimulation (L-proline concentration modulation) show up in this demodulated spectrum. As a consequence, the contribution of adsorbed NAC is basically removed, except for periodic changes induced by the proline concentration modulation. However, besides the proline bands, other significant signals are apparent, notably the sharp small band at about 1674 cm^{-1} and a broad band at about 1732 cm^{-1}. The latter is assignable to the ν(–COOH) vibration of adsorbed NAC, whereas the former is likely due to the NAC amide I mode. Figure 4 shows that this band is shifted to higher wavenumber with respect to the bare NAC SAM. The fact that NAC vibrations show up in the demodulated spectrum and that the NAC amide I vibration has shifted, strongly suggests an interaction of proline with the NAC SAM.

The modulation technique allows species with different kinetics to be separated, by choosing the demodulation phase angle ϕ_k^{PSD} in Equation (1) (Experimental Section) accordingly. Therefore, if the dissolved and adsorbed proline have different kinetics, the contribution of the dissolved species would vanish at a certain demodulation phase angle, leaving only the spectrum of the adsorbed species. However, in the present case, the signals in the demodulated spectrum all had very similar phase behavior, that is, there was no significant phase lag between dissolved and adsorbed species. This in turn indicates that, on our time scale, dissolved and adsorbed proline are in equilibrium, and that this equilibrium is established fast. In summary, the spectral response to the L-proline concentration modulation in presence of the NAC SAM clearly indicates intermolecular interactions between selector (NAC) and selectand (proline). It should be noted that the analogous experiment with D-proline resulted in very similar spectra. In order to investigate differences in the interaction of the two proline enantiomers and the NAC SAM, absolute configuration modulation experiments were performed, which selectively highlights these differences. These experiments are discussed next.

In Figure 5 we present a series of phase-resolved spectra which refer to absolute configuration modulation experiments. In these experiments, using a modulation period of $T = 362.3$ s and a flow rate of 0.18 mL min^{-1}, the absolute configuration of proline was changed periodically by flowing the two enantiomers over the NAC SAM, starting with an inflow of D-proline. Again, it should be noted that only bands that are periodically changing with time, owing to the stimulation (absolute proline configuration modulation), show up in these spectra. These spectra thus reveal the differences in intermolecular interactions between the two proline enantiomers and the NAC SAM. The strongest features in the spectrum are positive and negative bands between 1700 and 1550 cm^{-1}, particularly at 1667 cm^{-1} (negative), 1650 cm^{-1} (positive), 1630 cm^{-1} (positive, shoulder on the 1650 cm^{-1} band), at about 1600 cm^{-1} (negative, broad) and about 1550 cm^{-1} (positive, very broad). In addition, a weaker signal is observed at about 1375 cm^{-1}.

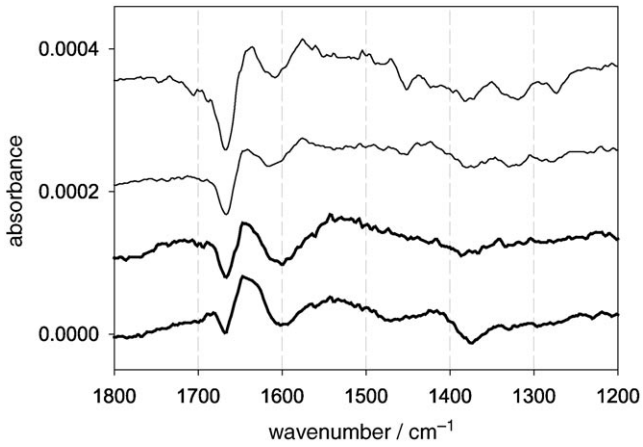

Figure 5. Demodulated spectra performed on different days using different gold-coated Ge IREs illustrating the repeatability of the absolute configuration modulation experiments (period $T = 362.3$ s, flow-rate 0.18 mL min^{-1}). Bottom) (——) D- and L-proline, (0.04 M) periodically flowed over NAC after two hours of self-assembly. Top) (——) The self-assembly of NAC on gold-coated Ge IRE was stopped after one minute, and deprotonation of adsorbed NAC molecules was followed until no spectral variation could be detected. Then D- and L-proline were allowed to flow alternately over the NAC SAM.

At this point, some general statements can be made: 1) The spectral response of the absolute configuration modulation experiments is rather complex, revealing positive and negative signals—the spectral response can therefore not be reduced to the strong adsorption of only one enantiomer, which would lead to spectra strongly resembling the proline spectrum. However, the contribution of different equilibrium coverages of the adsorbing enantiomers to the observed spectral response cannot be excluded completely, since, in general, the observed demodulated spectra are a combination of spectral differences due to enantiospecific interactions *and* coverage differences. The spectral response (positive and negative bands) still indicates that enantiospecific effects dominate over coverage effects. 2) As also mentioned in the Experimental Section, control experiments with proline and the gold-coated Ge IRE (that is, in the absence of the NAC SAM) revealed that the signals in Figure 5 are not due to proline interacting with the bare gold surface. 3) The signals due to intermolecular interactions are more than one order of magnitude smaller than the spectrum of NAC adsorbed on gold (compare to the NAC spectrum in the lower half of Figure 4). Still the signals are considerably above the noise level, which is about 5×10^{-6} in the spectral region around 1700 cm^{-1}. The strength of the signals thus suggests that the enantiodiscrimination between the NAC SAM and proline is rather weak and/or that the interaction between the SAM and proline is weak. In order to emphasize the significance of the results and reproducibility, a series of demodulated spectra is presented in Figure 5, referring to absolute configuration modulation experiments performed on different days using different gold-coated Ge IREs. Furthermore, different NAC-modified Au surfaces were probed by varying

the duration of the self- assembling process from two hours (2 h SAM) to one minute (1 min SAM). Note that in the case of the latter adsorbate layer, the subsequent deprotonation was completed about thirty minutes before modulation experiments were performed. The two spectra at the bottom in Figure 5 (——) refer to the 2 h SAM (different experiments!), whereas the two spectra depicted on top (——) refer to the 1 min SAM (again different experiments). The reproducibility of the spectral response for each of the two differently modified surfaces (2 h and 1 min SAM) is good (compare the two pairs of traces with —— and ——). But, there is also a remarkable similarity in the spectra for the 2 h and 1 min NAC SAM. This shows that the interactions responsible for the observed spectral changes are the same for the two SAMs, although the NAC coverage and also the long-range ordering, is largely different in the two cases. This, in turn, indicates that the interaction between proline and the SAM is a 1:1 type interaction, that is, an interaction between a proline molecule and one individual adsorbed NAC molecule (as opposed to an ordered "supramolecular" NAC agglomerate on the gold surface). Furthermore, in a control experiment, NAC deprotonation on the surface was inhibited by the addition of 0.013 M HCl, which was verified by the absence of corresponding carboxylate vibrational bands. A following absolute configuration modulation experiment (in the presence of HCl, 0.013 M) showed a completely different spectral response with significantly weaker signals due to the different kind of interactions (ion–dipole, dipole–dipole, etc.) in this case. Note that in these experiments, proline is protonated at the acid group.

Dispersive bands in demodulated spectra, such as the ones observed for the absolute configuration modulation experiments (Figure 5), can arise due to slight frequency shifts induced by the stimulation. In our case, this means that, owing to the different interactions between the enantiomers of proline and the chiral SAM, the spectrum of the interaction complex changes slightly. Note that no such changes, and therefore no signals, are expected in the demodulated spectra for an absolute configuration modulation experiment over a nonchiral surface.[34] The position of the dispersive bands suggests frequency shifts of the proline carboxylate $\nu_{as}(COO^-)$ (possibly also $\nu_s(COO^-)$) and NH_2 scissoring $\delta(-NH_2)$ and NAC amide and carboxylate vibrations (see corresponding spectra in the lower half of Figure 4). The demodulated spectrum of the "L-proline versus ethanol" experiment (Figure 4, top, ——) indeed shows an NAC amide I band (at 1674 cm^{-1}) that is shifted owing to interactions with proline. On the other hand, the same spectrum also reveals a small ν(COOH) band associated with protonated NAC, whereas no clear sign of such a band is visible in the demodulated spectra of the absolute configuration modulation experiments (Figure 5). This indicates that protonated NAC on the surface also interacts with proline, but that this interaction is not enantiospecific. In a more general sense, this finding shows that both enantiospecific and nonspecific interactions take place at the chiral SAM, and it indicates that it is the deprotonated NAC that is involved in the enantiospecific interaction. In order to understand the origin of the observed dispersive bands in Figure 5 better, DFT calculations on the interaction between NAC and proline have been performed, and will be discussed in the next section.

Calculated IR Spectrum of a D(L)-Proline–NAC Complex

In Figure 6 we present the calculated IR spectra of zwitterionic proline, anionic *N*-acetyl-L-cysteine, and the NAC–proline complex (see Figure 3 for the structure). The calculated spectra were obtained from the optimized structures of the corresponding conformations. All of these spectra were obtained by convoluting the corresponding calculated IR intensities with a Lorentzian band shape ($\gamma = 10$ cm^{-1}). In Figure 6, the most important vibrational bands used for the following discussion are labeled. Some of the prominent vibrational bands of proline and NAC undergo considerable frequency shifts upon complexation, as is obvious from Figure 6. Specifically, the proline $\nu_{as}(-COO^-)$ band shifts about 15 cm^{-1} to lower wavenumbers, whereas the δ_s $(-NH_2)$ scissoring vibrational band shifts about 42 cm^{-1} up in the NAC-proline complex. NAC band shifts are visible for the $\nu_{as}(-COO^-)$ and amide I bands, which results in a single, strong asymmetric band in the vibrational spectrum of the complex. Careful inspection further shows that the amide II and methyl bands slightly shift (by about 6 cm^{-1}) to higher frequencies. The calculations show that the intense band of the complex between about 1250 and 1380 cm^{-1} consists of sever-

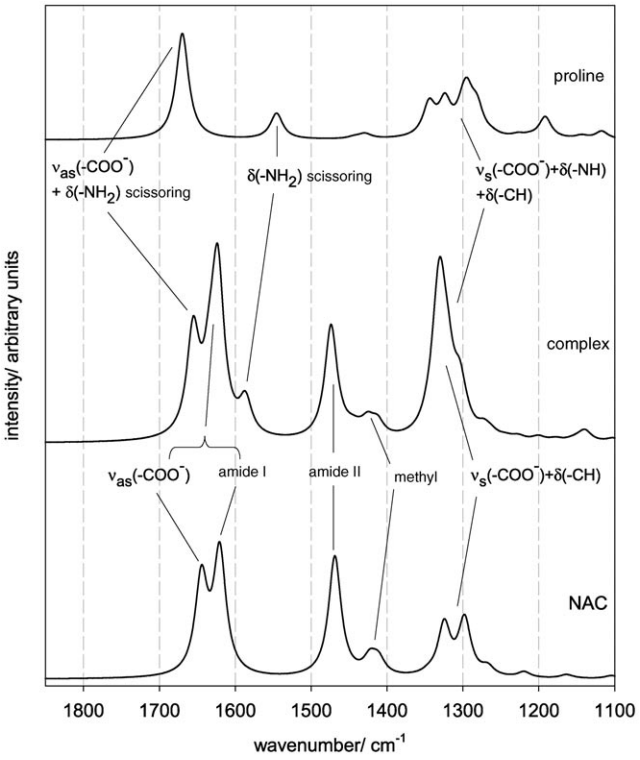

Figure 6. Calculated IR spectra of zwitterionic proline, anionic NAC, and the NAC–proline complex [IR intensities convoluted with a Lorentzian band shape ($\gamma = 10$ cm^{-1})] . The prominent vibrational bands of the corresponding species are labeled (see Table 1 for frequency calculation).

al complex vibrational modes, notably proline ν_s(–COO^-) + δ(–NH) + δ(–CH) and NAC ν_s(–COO^-) + δ(–CH).

As already mentioned above, the calculations strongly indicate that the interaction between anionic NAC and zwitterionic proline is largely determined by charge–charge interactions, that is attraction between the positive nitrogen of proline and the negative carboxylate of NAC, as well as repulsion between the negative carboxylates of proline and NAC (Figure 3). In an optimal arrangement of these charges, an additional intermolecular interaction is established, namely a proline–NH_2^+···OOC^-–NAC hydrogen bond. A direct comparison of the calculated and experimental spectra of the complex is difficult, since our experiments do not yield the direct experimental counterpart of the complex spectrum in Figure 6. What is experimentally accessible, via the proline concentration modulation over the NAC SAM (Figure 4, top, ——), is a superposition of 1) the spectrum of the complex on the surface (including changes of the NAC spectrum induced by complex formation) and 2) the spectrum of dissolved proline, the latter being considerably stronger. Still, a couple of observations support a complex structure as predicted by the DFT calculations (Figure 3): 1) The calculations predict a blue shift of the NAC amide I band upon complexation, as is observed in the experimental spectrum (band at 1674 cm^{-1} in Figure 4, top, ——). 2) The calculations predict a red shift in the proline carboxylate vibration ν_{as}(COO^-). The comparison between the ATR-IR spectrum of the dissolved proline (Figure 4, bottom, ——) and the demodulated spectrum of the "L-proline versus ethanol" modulation experiment (Figure 4, top, ——) reveals a broadening of the proline ν_{as}(COO^-) band at about 1637 cm^{-1} towards lower wavenumbers upon interaction with the NAC SAM. This shows that for the adsorbed species the ν_{as}(COO^-) has shifted to lower wavenumbers, as predicted by the calculations. 3) Upon complex formation, a rather dominant band is predicted in the spectral region of the ν_s(COO^-) bands of NAC and proline (calculated at about 1340 cm^{-1}, observed at about 1400 cm^{-1}) and that the ν_s(COO^-) bands are shifting to higher wavenumbers. The comparison between the ATR-IR spectrum of the dissolved proline (Figure 4, bottom, ——) and the demodulated spectrum of the "L-proline versus ethanol" modulation experiment (Figure 4, top, ——) indeed shows increased intensity slightly above 1400 cm^{-1}, thus supporting the calculated structure.

Finally, the absolute configuration modulation experiments (Figure 5) resulted in several dispersive bands in the spectrum due to frequency shifts, indicating that the position of the vibrational bands of the NAC–proline complex depends on the absolute configuration of proline. Note that the spectra in Figure 5, that is, the result of the absolute configuration modulation experiments, can be viewed as difference spectra between the NAC–D-proline and the NAC–L-proline complexes. The analogous difference spectrum can also be derived from the DFT calculations. The result of the vibrational analysis for the NAC–D-proline complex, denoted by "(D)" and the NAC-L-proline complex, denoted by "(L)" together with the corresponding difference spectrum (——, "L−D") is displayed in Figure 7. Note: the reason for calculating the difference spectrum in the order "(L)−(D)" and not "(D)−(L)" follows from the demodulated ATR-IR spectra of the "D versus L-proline" absolute configuration modulation experiment (starting with an inflow of D-proline) which showed maximum amplitude for demodulation phase angles ϕ_k^{PSD} around 170° (for demodulation angles differing by 180° the resulting demodulated spectra are identical, but for the sign of all absorption bands). At first glance, the calculated spectra of the (D) and (L) complex seem almost identical, but the resulting difference spectrum, scaled by a factor of five, clearly reveals significant dispersive bands that originate from slight frequency shifts of vibrational bands, notably in the region of 1560 to 1680 cm^{-1} and 1470 cm^{-1}. The former bands are related to proline ν_{as}(–COO^-) and δ_s(–NH_2) as well as NAC ν_{as}(–COO^-) and amide I bands, whereas the latter mainly originates from the NAC amide II vibrational band. The calculated frequency shifts between the bands of the NAC–D-proline and NAC–L-proline complexes are of the order of only one wavenumber for most of the important bands, and about four wavenumbers for the proline δ_s (–NH_2) scissoring mode. As can be further seen, the calculated frequency shift for the broad band between about 1250 and 1380 cm^{-1} containing complex modes is rather small. From the calculated difference spectrum in Figure 7 and the experimental counterpart, several interesting points emerge. The calculations clearly show that very small frequency shifts of the complex due to the change of the absolute configuration of proline result in significant dispersive and broad features in the corresponding difference spectrum. This means that absolute configuration modulation experiments, as performed here, are very sensitive to such small changes and are thus very sensitive to spotting small differences in diastereomeric interactions.

The dispersive bands in the region of 1650 cm^{-1} in the experimental spectrum imply a small shift in the proline ν_{as}(COO^-) and δ_s(NH_2) scissoring modes, as well as the NAC

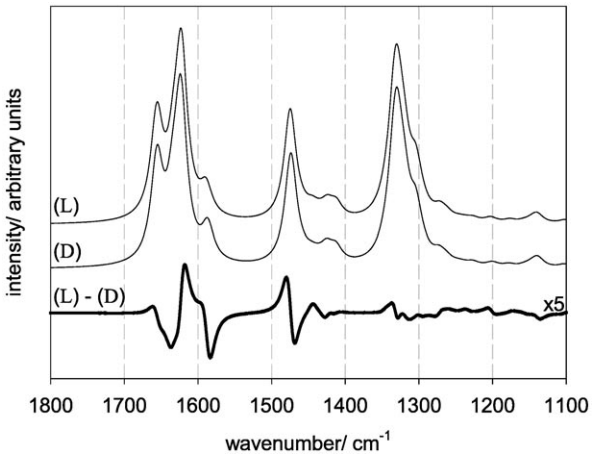

Figure 7. Top) Calculated vibrational spectra (of optimized structures from Figure 3) of NAC–D-proline ("D") and NAC–L-proline ("L") complexes [IR intensities convoluted with a Lorentzian band shape (γ = 10 cm^{-1})]. The assignment of the prominent vibrational bands is given in Figure 6. Bottom) Calculated difference (L)–(D) spectrum (——) between NAC–L-proline and NAC–D-proline complex (scaled by a factor of five). Note that the calculated difference spectrum is experimentally accessible by ATR-IR (Figure 5).

amide I mode, which is in good agreement with the calculations. Furthermore, the broad band at about 1540 cm^{-1} appearing in the experimental spectrum (Figure 5) is probably related to a shift of the NAC amide II band (see the NAC spectrum in Figure 4) which is also supported by the DFT calculations (dispersive band calculated at about 1470 cm^{-1} in Figure 7). Possibly the weak band around 1400 cm^{-1} in the experimental spectrum (Figure 5) is associated with a shift of the ν_s(–COO^-) carboxylate vibrations. A weak signal due to slight shifts of ν_s(–COO^-) is also predicted by the calculations. In summary, the calculations based on the complexes in Figure 3 are in qualitative agreement with experiment. In particular, the dispersive line pattern observed between 1550 and 1700 cm^{-1} is very well reproduced by the calculations.

It should be noted that the calculated structures in Figure 3 exhibit certain rigidity along the axis defined by the three charges (see Figure 3) due to the electrostatics. However, the complexes are certainly still rather flexible, as the interaction is basically a "one point interaction" (neglecting the surface). This flexibility is not included in the calculations, which rely on potential minima. The fact that the interaction is basically only a "one point interaction" is consistent with the very small calculated energy difference between the two diastereomeric complexes, which is also consistent with experiment. Still, even such weakly enantiodiscriminating interactions lead to detectable signals in the difference spectrum of the two diastereomeric complexes, as revealed by absolute configuration modulation.

A further interesting point is the comparison between SAMs of NAC and L-GSH with respect to enantiodiscrimination. As already mentioned in the Introduction, the GSH SAM was found to discriminate well between proline enantiomers, with D-proline being more strongly bound. The spectra furthermore indicated pronounced structural changes within the GSH SAM upon interaction with proline. In contrast, the NAC spectra revealed merely slight frequency shifts only, which indicates that the NAC conformation does not drastically change upon interaction. The reason for the better enantiodiscrimination of GSH may therefore be associated with its larger flexibility as compared to NAC.

Conclusions

The enantiodiscrimination between NAC self-assembled on gold (selector) and the analyte molecule proline (selectand, dissolved in ethanol) was probed by in situ ATR-IR MES. In particular, by modulating the absolute configuration of proline over the chiral SAM, the differences in the diastereomeric interactions between the enantiomers of the selectand and the selector can be spotted. The resulting demodulated spectra showed weak, but significant and characteristic, dispersive bands.

The ATR spectra of the NAC SAM, in the absence of proline, show that protonated and deprotonated (at the acid group) forms coexist on the surface. Whereas the protonated form is influenced by the presence of proline, only the deprotonated form leads to enantiodiscrimination. The spectral response in the absolute configuration modulation experiments was found to be very similar for SAMs that were assembled for only 1 min and SAMs that were assembled for 2 h, which points to a 1:1 interaction between proline and an adsorbed NAC molecule being responsible for the observed enantiodiscrimination rather than a supramolecular assembly of NAC molecules.

DFT calculations on the proline (zwitterionic)–NAC (anionic) complex showed that the Coulomb interaction between the charges on the two counterparts determines the structure of the complex together with a hydrogen bond between the NH_2 group of proline and the carboxylate of NAC. The vibrational analysis of the optimized structure of the complex, including solvent (ethanol) effects, revealed significant shifts in prominent vibrational bands upon interaction, notably of the amide, carboxylate, and NH_2 modes, which are consistent with the experimental observations. The calculated spectra of the two diastereomeric complexes between NAC and proline enantiomers were very similar, and the energy difference between the two complexes was only small. However, the difference spectrum still revealed significant dispersive bands, owing to slightly different band positions, of the order of only one to a few wavenumbers, for the two diastereomeric complexes. The dispersive bands in the difference spectrum were mainly related to shifts in the proline ν_{as}(–COO^-) and δ_s(–NH_2) scissoring, as well as the NAC amide vibrational bands. The calculated difference spectrum is directly comparable with the demodulated spectra obtained from an absolute configuration modulation experiment and qualitative agreement was observed. The calculations furthermore showed that the NAC–proline interaction is a "one point interaction", which explains the small energetic and spectral differences. These small differences can be spotted by absolute configuration modulation spectroscopy, since this technique selectively highlights differences and, as shown here, band shifts of the order of only one wavenumber result in significant dispersive bands in the difference spectrum between the two diastereomeric complexes.

Experimental Section

Chemicals: All the reagents, NAC (min. 99% TLC, Sigma–Aldrich Inc.), D- and L-proline (both > 99% Sigma–Aldrich, Inc.), were used as recieved. The solutions were prepared in ethanol (ethanol, Merck p.a.). Dissolved oxygen was removed by bubbling nitrogen gas (99.995%, CarbaGas) through the solutions before each ATR-IR measurement.

In Situ ATR-IR Spectroscopy: The IREs (Komlas) used for all ATR-IR experiments were 50 mm × 20 mm × 2 mm Ge trapezoids with an angle of incidence of 45°. The Ge IREs were polished with a 0.25 μm grain size diamond paste (Buehler, Metadi II) and afterwards rinsed copiously with ethanol before the surface was plasma-cleaned under a flow of air for 5 min (PlasmaPrep 2, Gala Instrumente). In a final step, a gold layer with a thickness of about 2 nm was sputtered onto the Ge IRE (Balzers Union SCD 030). For each ATR-IR experiment, a Ge IRE with a freshly prepared gold layer was used. Control experiments with a bare Ge IRE revealed no NAC adsorption during several hours of exposure to a corresponding solution.

Data Acquisition: The spectrometer used for ATR-IR measurements was a Bruker Equinox 55 Fourier transform infrared (FTIR) spectrometer equipped with a liquid-nitrogen-cooled narrow band mercury cadmium telluride (MCT) detector. The solutions, stored in separate bubble tanks, were introduced into a home-built liquid flow-through cell with a total volume of 0.077 mL leaving a gap of 250 μm between the IRE and the polished steel surface. A more detailed description of the ATR-IR cell can be found elsewhere.[33,45] All ATR-IR spectra reported herein were performed at room temperature (298 K) and were recorded with 4 cm^{-1} resolution at a 40 kHz sampling rate.

ATR-IR and Modulation Experiments: Typical ATR-IR (modulation) experiments started with an inflow of solvent (ethanol) over the gold-coated Ge IRE until no variation in the spectrum could be detected (after about 5 min). The corresponding background spectrum, recorded by co-adding 200 interferograms, served as the reference for all subsequent (modulation) experiments. In order to study the adsorption and self-assembling of NAC on gold, NAC dissolved in ethanol (about 0.6 mM for all ATR-IR measurements reported herein) was allowed to flow at 0.18 mL min^{-1} over the gold-coated Ge IRE. Spectral changes were followed in situ for up to two hours by recording spectra at time intervals of about 5 min. A solution ATR-IR spectrum of the analyte proline was obtained by performing a modulation experiment on a bare Ge IRE. The flow of L-proline dissolved in ethanol (0.04 M) during the first half period was replaced by an equally long flow of solvent (ethanol) during the second half period of the modulation experiment. An analogous modulation experiment was repeated with the gold-coated Ge IRE, in order to investigate the interaction of proline with the "bare" gold surface. For these modulation experiments, a period of $T = 120.7$ s at a flow rate of 0.5 mL min^{-1} was used. In order to study the intermolecular interactions between each of the two proline enantiomers and the NAC SAM, concentration modulation experiments were performed. D-proline (0.04 M) and ethanol were periodically flowed over the chiral NAC modified gold surface. An analogous modulation experiment was performed with the other enantiomer, L-proline, at the same concentration. These modulation experiments, denoted by "D(L)-proline versus ethanol", were performed using a modulation period of $T = 72.4$ s, and a flow rate of 0.5 mL min^{-1}. Finally, the enantioselective discrimination between the NAC SAM (selector) and the analyte molecule proline (selectand) was probed by an absolute configuration modulation experiment. In this experiment, denoted "D- versus L-proline", D- and L-proline (both at 0.04 M) were allowed to flow periodically over the NAC SAM, starting with an inflow of D-proline. Absolute configuration modulation experiments were performed using a modulation period of $T = 362.3$ s and a flow rate of 0.18 mL min^{-1}.

All of the modulation experiments reported herein consisted of two initial "dummy loops" to let the system reach a new, quasistationary state, followed by averaging over four measurement loops (periods). During one measurement period (loop), 60 infrared spectra were recorded at a 40 kHz sampling rate using the rapid scan acquisition mode of the FTIR spectrometer. For each spectrum, 6, 10, and 30 interferograms were averaged, resulting in modulation periods of $T = 72.4$, 120.7, and 362.3 s, respectively. A digital PSD according to Equation (1) was then used to transform a set of time-resolved spectra to phase-resolved spectra.

$$A_k^{\phi_k^{PSD}}(\tilde{\nu}) = \frac{2}{T}\int_0^T A(\tilde{\nu}, t)\sin(k\omega t + \phi_k^{PSD})dt \qquad (1)$$

where $k = 1,2,3,\ldots$ determines the demodulation frequency, that is, fundamental, first harmonic, and so on; T is the modulation period; $\tilde{\nu}$ denotes the wavenumber; ω the stimulation frequency; and ϕ_k^{PSD} the demodulation phase angle. With a set of time-resolved spectra $A(\tilde{\nu}, t)$, Equation (1) can be evaluated for different phase angles ϕ_k^{PSD} resulting in a series of phase-resolved spectra $A_k^{\phi_k^{PSD}}$. Only spectra demodulated at the fundamental frequency ($k = 1$) are reported here. A more detailed description of the modulation technique can be found elsewhere.[32,33,42]

DFT Calculations for *N*-Acetyl-L-cysteine and Proline: DFT calculations were performed using the hybrid functional B3PW91[46,47] with a 6–31G basis set.[48] GAUSSIAN03 was used for all calculations.[49] Solvent (ethanol) effects were accounted for by performing optimizations using a PCM.[50] Structure optimizations were performed for neutral (uncharged) NAC and the zwitterionic form of proline, since these prevail in ethanol. For reasons that are discussed in the Results and Discussion Section, structure optimization and vibrational analysis was also performed for NAC in the deprotonated state, that is, in the anionic form. Finally, the interaction complexes between NAC (anionic) and the two proline enantiomers were considered at the same level of theory. More computational details are given in the Results and Discussion Section.

Acknowledgements

Financial support from the Swiss National Science Foundation and grants of computer time from the Swiss National Supercomputing Centre (CSCS) Manno are gratefully acknowledged. The use of sputtering facilities at the Swiss Center for Electronics and Microtechnology in Neuchâtel (CSEM) is kindly acknowledged.

Keywords: chirality · density functional calculations · enantioselectivity · IR spectroscopy · self-assembly

[1] S. Ahuja, *Chiral Separations by Chromatography*, Oxford University Press, Washington, DC, **2000**.
[2] T. Bürgi, A. Baiker, *Acc. Chem. Res.* **2004**, *37*, 909.
[3] D. Y. Murzin, P. Maki-Arvela, E. Toukoniitty, T. Salmi, *Catal. Rev.—Sci. Eng.* **2005**, *47*, 175.
[4] C. F. McFadden, P. S. Cremer, A. J. Gellman, *Langmuir* **1996**, *12*, 2483.
[5] J. D. Horvath, A. J. Gellman, *J. Am. Chem. Soc.* **2002**, *124*, 2384.
[6] J. D. Horvath, A. Koritnik, P. Kamakoti, D. S. Sholl, A. J. Gellman, *J. Am. Chem. Soc.* **2004**, *126*, 14988.
[7] R. M. Hazen, D. S. Sholl, *Nat. Mater.* **2003**, *2*, 367.
[8] G. A. Attard, *J. Phys. Chem. B* **2001**, *105*, 3158.
[9] M. O. Lorenzo, C. J. Baddeley, C. Muryn, R. Raval, *Nature* **2000**, *404*, 376.
[10] M. O. Lorenzo, S. Haq, T. Bertrams, P. Murray, R. Raval, C. J. Baddeley, *J. Phys. Chem. B* **1999**, *103*, 10661.
[11] D. Ferri, T. Bürgi, *J. Am. Chem. Soc.* **2001**, *123*, 12074.
[12] N. Bonalumi, T. Bürgi, A. Baiker, *J. Am. Chem. Soc.* **2003**, *125*, 13342.
[13] M. Schunack, E. Laegsgaard, I. Steengaard, I. Johannsen, F. Besenbacher, *Angew. Chem.* **2001**, *113*, 2693; *Angew. Chem. Int. Ed.* **2001**, *40*, 2623.
[14] A. Kühnle, T. R. Linderoth, B. Hammer, F. Besenbacher, *Nature* **2002**, *415*, 891.
[15] K.-H. Ernst, Y. Kuster, R. Fasel, M. Müller, U. Ellerbeck, *Chirality* **2001**, *13*, 675.
[16] R. Fasel, J. Wider, C. Quitmann, K. H. Ernst, T. Greber, *Angew. Chem.* **2004**, *116*, 2913; *Angew. Chem. Int. Ed.* **2004**, *43*, 2853.
[17] D. S. Sholl, *Langmuir* **1998**, *14*, 862.
[18] D. Stacchiola, L. Burkholder, W. T. Tysoe, *J. Mol. Catal A: Chem.* **2004**, *216*, 215.
[19] P. Messina, A. Dmitriev, N. Lin, H. Spillmann, M. Abel, J. V. Barth, K. Kern, *J. Am. Chem. Soc.* **2002**, *124*, 14000.
[20] R. B. Rankin, D. S. Sholl, *Surf. Sci.* **2004**, *548*, 301.
[21] R. B. Rankin, D. S. Sholl, *Surf. Sci.* **2005**, *574*, L1.

[22] R. B. Rankin, D. S. Sholl, *J. Phys. Chem. B* **2005**, *109*, 16764.
[23] R. McKendry, M.-E. Theoclitou, T. Rayment, C. Abell, *Nature* **1998**, *391*, 566.
[24] T. Nakanishi, N. Yamakawa, T. Asahi, T. Osaka, B. Ohtani, K. Uosaki, *J. Am. Chem. Soc.* **2002**, *124*, 740.
[25] K. Bodenhöfer, A. Hierlemann, J. Seemann, G. Gauglitz, B. Koppenhoefer, W. Göpel, *Nature* **1997**, *387*, 577.
[26] R. M. Hazen, T. R. Filley, G. A. Goodfriend, *Proc. Nat. Acad. Sci. USA* **2001**, *98*, 5487.
[27] D. A. M. Zaia, *Amino Acids* **2004**, *27*, 113.
[28] M. Kauranen, T. Verbiest, J. J. Maki, A. Persoons, *J. Chem. Phys.* **1994**, *101*, 8193.
[29] J. M. Hicks, T. Petralli-Mallow, *Appl. Phys. B: Lasers Opt.* **1999**, *68*, 589.
[30] I. Yagi, M. Chiba, K. Uosaki, *J. Am. Chem. Soc.* **2005**, *127*, 12743.
[31] N. J. Harrick, *Internal Reflection Spectroscopy*, Interscience Publishers, New York, **1967**.
[32] D. Baurecht, U. P. Fringeli, *Rev. Sci. Instrum.* **2001**, *72*, 3782.
[33] T. Bürgi, A. Baiker, *J. Phys. Chem. B* **2002**, *106*, 10649.
[34] R. Wirz, T. Bürgi, A. Baiker, *Langmuir* **2003**, *19*, 785.
[35] R. Wirz, T. Bürgi, W. Lindner, A. Baiker, *Anal. Chem.* **2004**, *76*, 5319.
[36] B. Ohtani, A. Shintani, K. Uosaki, *J. Am. Chem. Soc.* **1999**, *121*, 6515.
[37] T. Nakanishi, N. Yamakawa, T. Asahi, N. Shibata, B. Ohtani, T. Osaka, *Chirality* **2004**, *16*, S36.
[38] M. Bieri, T. Bürgi, *J. Phys. Chem. B* **2005**, *109*, 10243.
[39] T. Helgaker, E. Eggerud, H. J. A. Jensen, *Chem. Phys. Lett.* **1990**, *173*, 145.
[40] M. Dewar, W. Thiel, *J. Am. Chem. Soc.* **1977**, *99*, 4499.
[41] M. Bieri, T. Bürgi, *J. Phys. Chem. B* **2005**, *109*, 10243.
[42] M. Bieri, T. Bürgi, *Langmuir* **2005**, *21*, 1354.
[43] E. M. Marti, C. Methivier, C. M. Pradier, *Langmuir* **2004**, *20*, 10223.
[44] A. Pintar, R. Malacea, C. Pinel, G. Fogassy, M. Besson, *Appl. Catal. A* **2004**, *264*, 1.
[45] A. Urakawa, R. Wirz, T. Bürgi, A. Baiker, *J. Phys. Chem. B* **2003**, *107*, 13061.
[46] A. D. Becke, *J. Chem. Phys.* **1993**, *98*, 5648.
[47] J. P. Perdew, J. A. Chevary, S. H. Vosko, K. A. Jackson, M. R. Pederson, D. J. Singh, C. Fiolhais, *Phys. Rev. B* **1992**, *46*, 6671.
[48] R. Ditchfield, W. J. Hehre, J. A. Pople, *J. Chem. Phys.* **1971**, *54*, 724.
[49] M. J. Frisch, G. W. Trucks, H. B. Schlegel, G. E. Scuseria, M. A. Robb, J. R. Cheeseman, J. A. Montgomery, T. Vreven, K. N. Kudin, J. C. Burant, J. M. Millam, S. S. Iyengar, J. Tomasi, V. Barone, B. Mennucci, M. Cossi, G. Scalmani, N. Rega, G. A. Petersson, H. Nakatsuji, M. Hada, M. Ehara, K. Toyota, R. Fukuda, J. Hasegawa, M. Ishida, T. Nakajima, Y. Honda, O. Kitao, H. Nakai, M. Klene, X. Li, J. E. Knox, H. P. Hratchian, J. B. Cross, C. Adamo, J. Jaramillo, R. Gomperts, R. E. Stratmann, O. Yazyev, A. J. Austin, R. Cammi, C. Pomelli, J. W. Ochterski, P. Y. Ayala, K. Morokuma, G. A. Voth, P. Salvador, J. J. Dannenberg, V. G. Zakrzewski, S. Dapprich, A. D. Daniels, M. C. Strain, O. Farkas, D. K. Malick, A. D. Rabuck, K. Raghavachari, J. B. Foresman, J. V. Ortiz, Q. Cui, A. G. Baboul, S. Clifford, J. Cioslowski, B. B. Stefanov, G. Liu, A. Liashenko, P. Piskorz, I. Komaromi, R. L. Martin, D. J. Fox, T. Keith, M. A. Al-Laham, C. Y. Peng, A. Nanayakkara, M. Challacombe, P. M. W. Gill, B. Johnson, W. Chen, M. W. Wong, C. Gonzalez, J. A. Pople, Rev. C.01 ed., Gaussian, Inc., Wallingford CT, **2003**.
[50] M. T. Cancès, B. Mennucci, J. Tomasi, *J. Chem. Phys.* **1997**, *107*, 3032.